

The Attitude Determination and Control System of the Picosatellite UWE-3*

F. Reichel, P. Bangert
S. Busch, K. Ravandoor, K. Schilling *

* University Würzburg, Germany (e-mail:
schi@informatik.uni-wuerzburg.de)

Abstract: The picosatellite UWE-3 is the third generation of CubeSats at the University Würzburg. It is equipped with all necessary satellite systems, among them an advanced attitude determination and control system (ADCS), which will enable the satellite to determine its orientation in space in real-time and, within its actuator capabilities, to control and change this attitude. The hard- and software of the ADCS are described, as well as experiments performed with dedicated test setups, and the obtained results are presented.

Keywords: small satellites, attitude determination, sensor fusion, attitude control, formation flying, decision making and autonomy

1. INTRODUCTION

The picosatellite UWE-3 (University Würzburg Experimental satellite) is the third generation of a series of 1-unit CubeSats and will be the base for future satellite missions at University Würzburg (Busch and Schilling, 2012). UWE-3 is therefore equipped with all necessary satellite systems, among them an advanced attitude determination and control system (ADCS). It is the primary goal of UWE-3 to further develop a reliable, accurate and autonomous ADCS for picosatellites, which would be another important milestone for the realization of picosatellite formation flying (Schmidt and Schilling, 2010). The ADCS will enable the satellite to determine its orientation in space on-board and, within its actuator capabilities, to control and change its attitude.

The attitude determination is based on sun-sensors, magnetometers and gyroscopes. The sensor data is fused in an Isotropic Kalman Filter (IKF) where it is compared to theoretical models to estimate the current attitude in real time on board of UWE-3.

The attitude control system (ACS) of UWE-3 is based on magnetic torquers and a miniature reaction wheel. The actuators are used to stabilize the picosatellite and to perform attitude control maneuvers, commanded by various implemented control algorithms.

The UWE-3 system comprises a complete new system architecture for very small satellites (Busch and Schilling, 2012), with a main focus on flexibility and modularity. Nevertheless, UWE-3 is equipped with the same main subsystems as a conventional satellite. Fig. 1 shows the modular structure of UWE-3 with its subsystems and the six side panels with attached solar cells.

* The UWE-3 project is funded by the German Aerospace Center (DLR) with funding by the Federal Ministry of Economics and Technology, following a decision of the German Bundestag, grant number 50 RU 0901

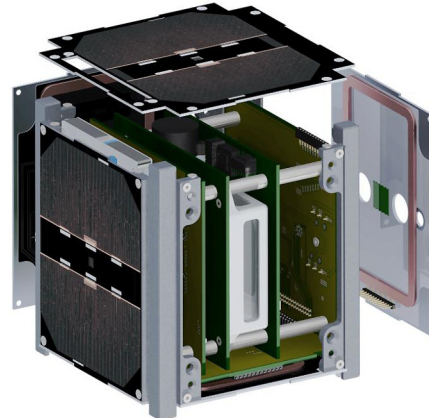


Fig. 1. Modular structure of UWE-3.

2. ADCS HARDWARE

This section describes the hardware used on-board the ADCS of UWE-3. This includes the sensor suite for attitude determination and the actuator suite for attitude control. Special focus will be put on the design and the performance of these highly integrated parts.

2.1 Attitude Determination Hardware

The UWE-3 sensor suit consists of in total nine single-axis magnetometers, three single-axis MEMS¹ gyroscopes and six two-angle sun-sensors. The sensor data from the three different sensor types is acquired separately and asynchronously and is post-processed to account for sensor specific calibration. This calibration is done on ground using an extensive calibration procedure further explained in Kiefel et al. (2011).

¹ Micro-Electro-Mechanical System

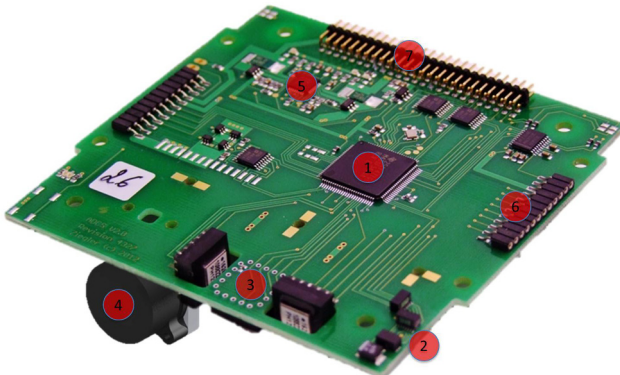


Fig. 2. The Attitude Determination and Control System of UWE-3: 1) Micro-controller, 2) magnetometers, 3) gyroscopes, 4) miniature reaction wheel, 5) hot-swap controller, 6) programming interface, 7) backplane connector

Magnetometer The Hall-effect based magnetometers are divided into a primary set of three magnetometers located directly on the ADCS PCB resembling a 3D compass, and secondary magnetometers placed on each side-panel. The attitude determination is based on the primary magnetometers with the secondary set provided for redundancy reasons. Although located inside the CubeSat, the precision of the 3D compass has been proven to be better than 3 deg. The secondary set of magnetometers is available for the attitude determination but has primarily been used for magneto-torquer verification.

Gyroscopes The gyroscopes can measure the satellite's angular velocity up to 320 deg/sec with a resolution of 0.073 deg/sec. The typical noise of the gyroscopes is 0.15 deg/sec, however they experience temperature related drifts. Therefore, the gyroscope's bias is part of the estimated state vector. This resembles at the same time a type of "software-gyroscope" which means, that the satellite is able to detect its angular velocity purely based on the other's sensors data (see section 3.1.1).

The gyroscopes are the most power consuming piece of hardware of the attitude determination system which makes power saving measures necessary. This is done using a programmable sleep mode of the gyroscopes for an adjustable period of time.

Sun-sensors The sun-sensors are highly integrated pieces of hardware that measure in total four quantities:

- (1) angle α in the sensor's X-Z plane towards the brightest object in its FOV
- (2) angle β in the sensor's Y-Z plane towards the brightest object in its FOV
- (3) light intensity measured by a red sensitive photo diode
- (4) light intensity measured by a blue sensitive photo diode

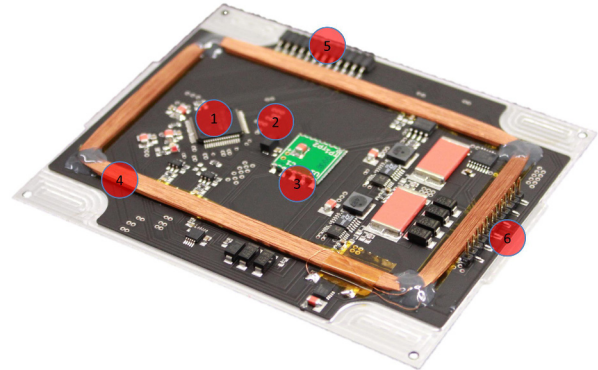


Fig. 3. The backside of a side panel: 1) Micro-controller, 2) magnetometer, 3) sunsensor, 4) magnetic torquer, 5) programming interface, 6) backplane connector

The sun-sensors have a 150 deg field of view (FOV), a resolution of the angles of 2.7 deg with an accuracy of 5 deg.

Since the sun-sensors measure angle and intensity separately, a light-source identification can be implemented based on the comparison of the two quantities (Bangert et al., 2012). In later use, also spectrum information containing the red to blue ratio might be used for albedo differentiation.

2.2 Attitude Control Hardware

The attitude control system of UWE-3 consists of two different actuation mechanisms. Each of the six side panels carries one magnetic torquer (MT), see Fig. 3. Additionally a miniature reaction wheel is mounted on the ADCS board as shown in Fig. 2.

Magnetic Torquer Magnetic control actuators have significant advantages compared to other attitude control mechanism. They are lightweight, require low power and are relatively inexpensive. Therefore, magnetic torquers are especially attractive for small satellites in low earth orbit (LEO). Another advantage of magnetic torquers is their high robustness since no moving parts are involved and the custom design possibilities. Due to the nature of interaction between the torquer magnetic moment and the Earth magnetic field, compare (1), no control torque can be produced along the instantaneous Earth magnetic field vector. However, for a time varying magnetic field as experienced on-board the satellite, this under-actuation problem can be resolved.

We designed and manufactured the magnetic torquers for the picosatellite UWE-3 to optimize power consumption, mass and the produced magnetic moment. The magnetic torquers for the flight- and flight-spare-model of UWE-3 are shown in Fig. 4. The parameters of the final magnetic torquer design are summarized in table 1.

The magnetic torquers produce a total maximum magnetic moment of $\mu_{max} = 0.1 \text{ Am}^2$, which results in a maximum torque, produced by the magnetic torquers of

$$|\mathbf{T}_{max}| = |\boldsymbol{\mu}_{max} \times \mathbf{B}_{max,earth}| = 4.6 \cdot 10^{-6} \text{ Nm}, \quad (1)$$

for a maximum Earth magnetic field of $B_{max} = 46 \mu\text{T}$.

This torque is 2-3 orders of magnitude higher than the expected disturbance torques due to the orbit environment. This ensures a successful application of the designed magnetic torquers for satellite stabilization and other attitude control maneuvers.

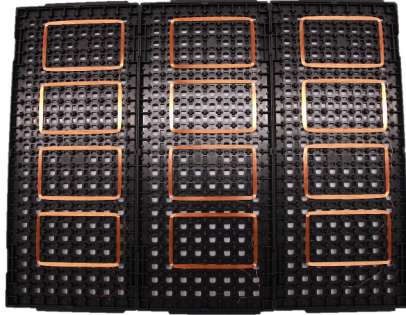


Fig. 4. The magnetic torquer for the UWE-3 flight model.

Table 1. Final magnetic torquer design specifications.

Parameter	Value
Magnetic moment	$\pm 0.028 \text{ Am}^2$
Max Supply Voltage	3.8 V
Max Supply Current	22 mA
Max Power Consumption	81 mW
Coil resistance	176 Ω
Number of turns	300
Mass	5.8 g
Mean Dimensions	52 \times 85 \times 2 mm ³

Miniature Reaction Wheel In addition to the six magnetic torquers, UWE-3 is equipped with one miniature reaction wheel (Astrofein, 20/01/2013), which is mounted on the ADCS board as shown in Fig. 2. It can store an angular momentum of $5.8 \cdot 10^{-4}$ Nms at nominal speed (8000 rpm) and can produce a maximum torque of $2.3 \cdot 10^{-5}$ Nm, which is one magnitude larger than the maximum torque produced by the magnetic torquers.

The reaction wheel can be used to eliminate the underactuation nature of pure magnetic attitude control at a single point in time by orienting the reaction wheel axis along the Earth magnetic field vector. In this configuration the picosatellite has the ability to fully control its attitude in all three axes, with a combined control of magnetic torquers and the reaction wheel.

3. ADCS SOFTWARE

This section describes the software used on-board the ADCS of UWE-3. The sensor data is fused in an Isotropic Kalman Filter (IKF), which allows to autonomously determine the attitude of UWE-3 on-board the picosatellite.

The attitude control actuators can be commanded by different algorithms implemented on the ADCS subsystem. The ADCS can autonomously switch between control strategies depending on the current attitude state of UWE-3.

3.1 Attitude Determination Software

The attitude determination is based on the comparison of sensor data of different types with their respective reference models. This comparison and the necessary sensor data fusion is done with an Isotropic Kalman Filter (IKF) which outputs the current attitude state estimation. The reference models used for the attitude determination are dependent on the satellite's orbital position which is estimated by employing an SGP-4 propagator that requires the orbital parameters (TLE²) and the current time as inputs.

A complete overview of the system is shown in Fig. 5.

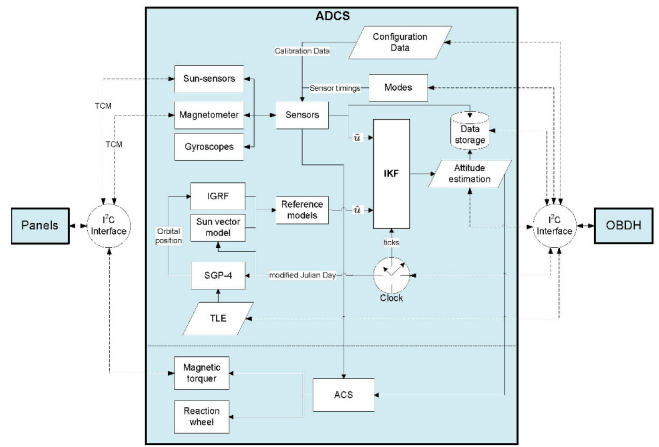


Fig. 5. Systematical overview of the Attitude Determination and Control System.

IKF The Isotropic Kalman Filter acts as the heart of the attitude determination system. It is used to estimate the satellite's attitude by performing sensor data fusion and the comparison of measured quantities with their respective models.

It was implemented for the Tropical Rainfall Measurement Mission (TRMM, Crassidis et al. (1995)) and adopted in previous works such as Kiefel et al. (2011). It was chosen with consideration of the limited computational power, the sensor accuracies as well as their update rate with respect to expected rotation rates of the satellite.

In the case of UWE-3, the attitude state vector \mathbf{x} contains the vector part of the quaternion \mathbf{q}_{vec} and a gyroscope bias vector \mathbf{b} . The gyroscope bias adjustment within the IKF detects rotations that are necessary to match all sensor measurements and which are not measured by the actual gyroscopes. These adjustments can become essential because the gyroscopes are expected to experience temperature shifts. On the other hand, they resemble a kind of "software-gyro", since rotations can be detected without the help of the actual gyroscopes.

As a recursive state estimation method, the IKF starts from a state \mathbf{x}_{k-1} and performs a prediction to a new state \mathbf{x}_k^- , using the dynamic model of the system. Then, this predicted new state is corrected by a measurement reading $\tilde{\mathbf{u}}$ and its corresponding reference vector $\hat{\mathbf{u}}$ to give the new state \mathbf{x}_k .

² Two Line Elements

The dynamic model of the system describes the propagation of the quaternion \mathbf{q}_{k-1} to \mathbf{q}_k^- as a rotation about the axis $\boldsymbol{\omega}_k$ measured by the gyroscopes and an angle $|\boldsymbol{\omega}_k| \cdot \Delta t$, where $\Delta t = t_k - t_{k-1}$ is the time elapsed between two subsequent measurements k and $k-1$.

The state correction from \mathbf{q}_k^- to \mathbf{q}_k is done using a measured vector $\tilde{\mathbf{u}}$ and a reference vector of the same type $\hat{\mathbf{u}}$. The reference vector is first transformed from its original coordinate frame by using the predicted attitude state \mathbf{q}_k^- . The innovation \mathbf{y}_k can be computed:

$$\mathbf{y}_k = \tilde{\mathbf{u}}_k \times \hat{\mathbf{u}}_k. \quad (2)$$

This correction is weighted by the Kalman gains $k_{q,k}$ and $k_{b,k}$ (defined further below) for the quaternion part and the bias part of the state vector respectively:

$$\delta \mathbf{q}_{vec,k} = \frac{1}{2} \cdot k_{q,k} \cdot \mathbf{y}_k \quad (3)$$

$$\Delta \mathbf{b}_k = k_{b,k} \cdot \mathbf{y}_k \quad (4)$$

Then it is applied to the predicted state $\mathbf{x}_k^- = (\mathbf{q}_k^-, \mathbf{b}_k^-)^T$ to give the new state estimation \mathbf{x}_k :

$$\mathbf{q}_k = \mathbf{q}_k^- * \left(\frac{\delta \mathbf{q}_{vec,k}}{\sqrt{1 - |\delta \mathbf{q}_{vec,k}|^2}} \right), \quad (5)$$

$$\mathbf{b}_k = \mathbf{b}_k^- + \Delta \mathbf{b}_k, \quad (6)$$

where $*$ denotes the quaternion multiplication.

The Kalman gains are closely coupled with the covariance which is dependent on the estimated noise parameters $\sigma_{\nu,1}$ and $\sigma_{\nu,2}$ and the noise level of the particular sensor measurement r .

The Kalman gain estimation again starts from the covariance of the previous state $k-1$, which is propagated into the new state:

$$p_{q,k}^- = p_{q,k-1} - 2p_{c,k-1}\Delta t + p_{b,k-1}\Delta t^2 + \sigma_{\nu,1}^2\Delta t + \frac{1}{3}\sigma_{\nu,2}^2\Delta t^3 \quad (7)$$

$$p_{c,k}^- = p_{c,k-1} - p_{b,k-1}\Delta t - \frac{1}{2}\sigma_{\nu,2}^2\Delta t^2 \quad (8)$$

$$p_{b,k}^- = p_{b,k-1} + \sigma_{\nu,2}^2\Delta t \quad (9)$$

where p_q , p_c and p_b are the covariance estimations for the quaternion part of the state vector, the correlation between the quaternion and the bias part, and the bias part itself, respectively. The Kalman gains are then computed by

$$k_{q,k} = \frac{p_{q,k}^-}{p_{q,k}^- + r} \quad (10)$$

$$k_{b,k} = \frac{p_{b,k}^-}{p_{q,k}^- + r} \quad (11)$$

using the estimated sensor noise r . The smaller the noise is, the higher the Kalman gains are, which means that this particular measurement would be trusted more. Also, regarding (3)–(6), it is apparent that this particular measurement would have a higher impact on the new state.

Then the covariance is corrected:

$$p_{q,k} = r \cdot k_{q,k} \quad (12)$$

$$p_{c,k} = r \cdot k_{b,k} \quad (13)$$

$$p_{b,k} = p_{b,k}^- - k_{b,k} \cdot p_{c,k}. \quad (14)$$

Software features The performance of the attitude determination is dependent on many different settings such as the update rate of each sensor. In accordance to its role as technical payload, the ADCS offers a wide range of adjustable parameters. For instance, there are different modes to obtain a sun-sensor threshold varying from a full autonomous threshold detection to a strictly preset threshold. Also for other sensors such as the gyroscopes, different modes exist to adjust their overall behavior e.g. with respect to power consumption.

Moreover, the ADCS features a data recording capability, which enables the user to record not only raw sensor data but also processed information such as the Kalman Filter's covariance and innovation, the current orbital position and velocity, or the reference model's outputs. This data recording makes use of the protected flash memory storage device on the On-board Data Handling System (OBDH) of the satellite.

3.2 Attitude Control Software

This section describes implemented attitude control algorithms used for stabilization and attitude control maneuvers. The most basic algorithm, which is used to detumble an initially spinning satellite is the B-Dot Controller.

B-Dot Controller In general, B-Dot control laws command a magnetic moment for each body axis, whose sign is opposite to that of the rate of change of the magnetic field measured in that axis. Thus, the generated torque is decreasing the rotational energy of the system. The most common B-Dot controller is a proportional $\dot{\mathbf{B}}$ control law, as described in Flatley et al. (1997), with a magnetic control moment of

$$\boldsymbol{\mu}_{ctrl} = -K\dot{\mathbf{B}} \quad (15)$$

where K is a positive gain factor and $\dot{\mathbf{B}}$ is the rate of change of the measured magnetic field. Thus, $\boldsymbol{\mu}_{x,ctrl} = -K\dot{B}_x$ activates the magnetic torquers along the body X-axis to damp the Y- and Z-components of the angular velocity.

Follow B-Field Controller The modified Follow B-Field algorithm can be used to keep the body Z-axis of UWE-3 (the reaction wheel spin axis) along the Earth magnetic field vector, so that the reaction wheel can be used to eliminate the under-actuation limitation of the magnetic torquers, as described before. Therefore, one magnetic torque along the body Z direction is continuously switched on, such that a constant magnetic moment in Z direction is produced. The X and Y magnetic torquers are used for damping and stabilization, thus they are controlled via the previously described B-Dot control law. The total Follow B-Field control law is given by

$$\boldsymbol{\mu}_{ctrl} = \begin{pmatrix} -K\dot{B}_x \\ -K\dot{B}_y \\ \mu_z \end{pmatrix}. \quad (16)$$

Combined Wheel Controller In case of a desired torque $\mathbf{T}_c = \mathbf{T}_B$ to be applied on the satellite, a control solution is described in Sidi (2000) using one reaction wheel in combination with magnetic torquers instead of using only magnetic actuators. As described before, the torque produced by the magnetic torquers can be written as

$$\mathbf{T}_B = \boldsymbol{\mu} \times \mathbf{B} = \begin{pmatrix} 0 & B_z & -B_y \\ -B_z & 0 & B_x \\ B_y & -B_x & 0 \end{pmatrix} \begin{pmatrix} \mu_x \\ \mu_y \\ \mu_z \end{pmatrix}. \quad (17)$$

However, the matrix in (17) can not be inverted to calculate the magnetic moment vector to be generated by the magnetic torquers. Introducing a reaction wheel instead of the magnetic actuator along the body Z-axis of the satellite, changes (17) to

$$\begin{pmatrix} T_{Bx} \\ T_{By} \\ T_{Bz} \end{pmatrix} = \begin{pmatrix} 0 & B_z & 0 \\ -B_z & 0 & 0 \\ B_y & -B_x & 1 \end{pmatrix} \begin{pmatrix} \mu_x \\ \mu_y \\ h_{wz} \end{pmatrix}, \quad (18)$$

where h_{wz} is the derivative of the wheel angular momentum, which is equivalent to the torque produced by the reaction wheel. Inverting the matrix in (18) gives the solution of the control equations

$$\begin{pmatrix} \mu_x \\ \mu_y \\ h_{wz} \end{pmatrix} = \frac{1}{B_z^2} \begin{pmatrix} 0 & -B_z & 0 \\ B_z & 0 & 0 \\ B_x B_z & B_y B_z & B_z^2 \end{pmatrix} \begin{pmatrix} T_{cx} \\ T_{cy} \\ T_{cz} \end{pmatrix}. \quad (19)$$

4. EXPERIMENTS AND RESULTS

The performance of the attitude determination and control system of UWE-3 has been tested and verified in various experiments. Therefore, special test setups have been developed and build by our workgroup. This section gives an overview about the available picosatellite test environments and presents the results of various verification experiments.

4.1 Attitude Determination Experiments

An attitude determination system testbed has been implemented in order to verify the system's response to various attitude scenarios. The testbed consists of a turntable (Kiefel et al., 2011), a computer directly connected to the hardware (via the programming interface, labeled as (6) in Fig. 2), and a narrow spotlight. The spotlight has been shown to emit parallel and homogenous light with respect to the sun-sensors accuracy. The test setup is shown in Fig. 6, where also the live representation of the computed attitude estimation is shown.

By placing the satellite in a known orientation onto the leveled turntable, the attitude calculated by the ADS can be compared to the actual orientation of the satellite. This is especially true for the vertical axis of the satellite, which will be assumed to be the pointing axis. The alignment of this axis with the laboratory's vertical can be measured and the angle between both gives an estimate for the accuracy of the attitude determination.

This alignment angle ("pointing error Z-axis", top) as well as the difference between the optical encoder and the estimated azimuth angle ("angle ϑ' ", bottom) are shown in Fig. 7 for the case of a non-rotating satellite. After initialization with a default attitude state, the pointing error is found to be 2.64 ± 0.8 deg after about 50 seconds.

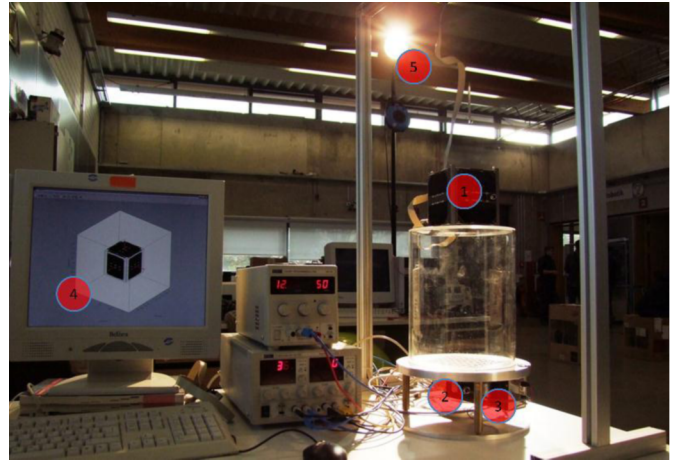


Fig. 6. Attitude determination testbed at the University of Würzburg: 1) UWE-3, 2) optical incremental encoder, 3) electric motor, 4) computer with live visualization, and 5) spotlight

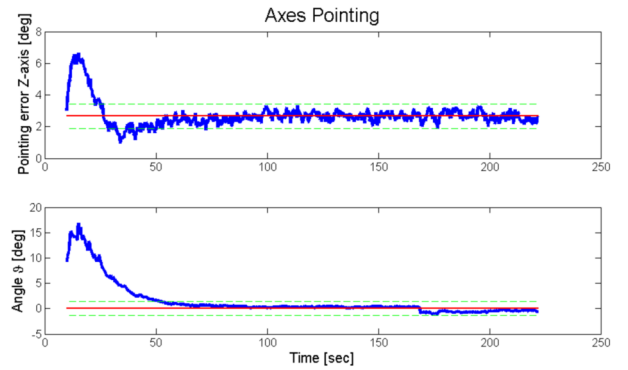


Fig. 7. Angle between laboratory Z-axis and the self-determined body Z-axis (top), and the error of the azimuth angle ϑ (bottom) during a steady state experiment. The dashed green lines indicate the 3σ variance and the solid red line the mean value.

The pointing accuracy of the system during a rotation of about 37 deg/sec about the pointing axis has been found to be 5.75 ± 2.76 deg and is shown in Fig. 8.

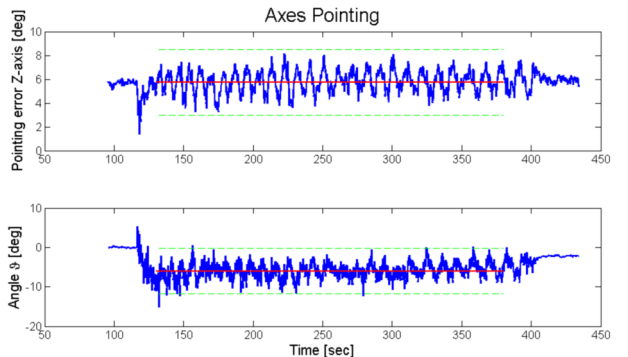


Fig. 8. Misalignment of the estimated Z-axis (top) and the azimuth angle ϑ (bottom) during spin at about 37 deg/sec.

During these experiments it became apparent, that there are some external causes for systematic errors which are

only expected to occur in the laboratory. For instance, it was found that the Earth's magnetic field, which is used for attitude determination also in the laboratory, is influenced significantly by the surrounding building which degrades the accuracy of the system. However, it has been proven that the attitude determination algorithm works consistently with the hardware and that the system is able to detect its orientation with an accuracy suitable for CubeSat applications.

4.2 Attitude Control Experiments

To perform attitude control experiments, a unique air cushion testbed for picosatellites has been designed and built, which allows to simulate force/torque free dynamics on ground. The CubeSat is mounted in a hollow acrylic sphere, which floats on a spherical air cushion bearing, as shown in Fig. 9.

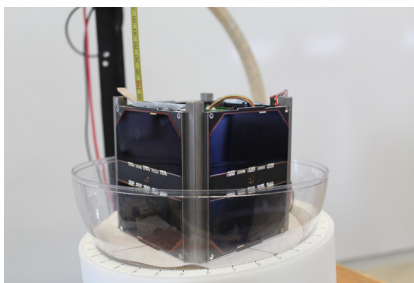


Fig. 9. Air cushion testbed for picosatellites with UWE-3 being mounted in an acrylic glass sphere.

Fig. 10 and Fig. 11 show the results of two stabilization experiments performed with the UWE-3 satellite on the air cushion testbed. In the first experiment, the satellite was initially spinning at $\omega_{init} \approx 65$ deg/s, mainly about its body Z-axis and it was able to stabilize after 325 seconds. In the second experiment, UWE-3 initially performed a random tumbling motion with an amplitude of $\omega_{init} \approx 40$ deg/s. With the applied stabilization control law, the satellite was stabilized after 450 seconds.

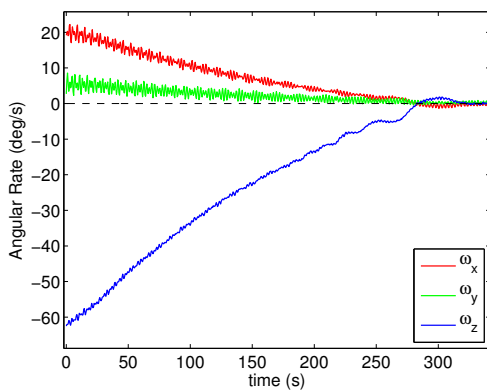


Fig. 10. The angular rate of the rotating satellite, measured with the ADCS gyroscopes during an UWE-3 despinning experiment.

Despite the fact that residual friction is apparent for all kind of ground experiments, the described setup and experiments show the successful implementation of the stabilization controller, verify the correct interaction between

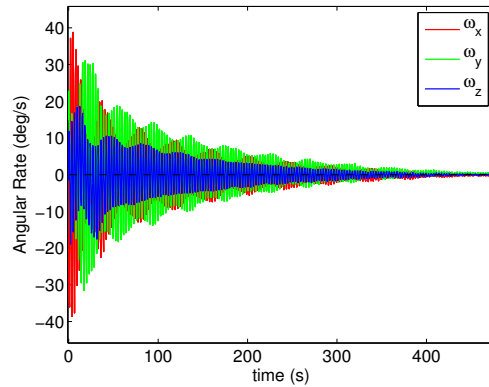


Fig. 11. The angular rate of the tumbling satellite, measured with the ADCS gyroscopes during an UWE-3 detumbling experiment.

attitude control hard- and software and show the successful use of the unique air cushion testbed for picosatellites.

5. CONCLUSION

The attitude determination and control system of UWE-3 is capable of determining the satellite's orientation in real time with an accuracy in the order of a few degrees. The control actuators can be used to control the attitude of the picosatellite. Performed experiments have shown the successful implementation of both hard- and software as well as the overall integration of the subsystem into the satellite.

REFERENCES

- Astrofein (20/01/2013). Astro- und Feinwerktechnik Adlershof GmbH. URL <http://www.astrofein.com>.
- Bangert, P., Reichel, F., Busch, S., and Schilling, K. (2012). Design- und Verifikationstests des Lageerkennungs- und Lageregelungssystems für den Picosatelliten UWE-3. Proceedings of the Deutscher Luft- und Raumfahrtkongress, Berlin.
- Busch, S. and Schilling, K. (2012). UWE-3: A Modular System Design for the Next Generation of Very Small Satellites. *Proceedings of Small Satellites Systems and Services - The 4S Symposium, Slovenia*.
- Crassidis, J., Andrews, S., and Markley, F. (1995). Contingency designs for attitude determination of TRMM. Technical report, Goddard Space Flight Center.
- Flatley, T., Morgenstern, W., Reth, A., and Bauer, F. (1997). A B-Dot Acquisition Controller for the RADARSAT Spacecraft. *Flight Mechanics Symposium*, (NASA-CP-3345), 79–89.
- Kiefel, P., Busch, S., Droege, W., and Schilling, K. (2011). Implementation, Calibration and Verification of a Kalman Filter based Attitude Determination System for the Picosatellite UWE-3. *GNC 2011, 8th International ESA Conference on Guidance, Navigation and Control Systems*.
- Schmidt, M. and Schilling, K. (2010). Formation flying techniques for pico-satellites. *6th International Workshop on Satellite Constellation and Formation Flying*.
- Sidi, M.J. (2000). *Spacecraft Dynamics and Control*. Cambridge University Press.